



# Scaling and intermittent properties of oceanic and atmospheric $p\text{CO}_2$ time series and their difference

Kévin Robache<sup>1</sup>, François G. Schmitt<sup>1</sup>, and Yongxiang Huang<sup>2,3</sup>

<sup>1</sup>Université du Littoral Côte d'Opale, Université de Lille, CNRS, Laboratoire d'Océanologie et Géosciences, Wimereux, France

<sup>2</sup>State Key Laboratory of Marine Environmental Science & Center for Marine Meteorology and Climate Change & College of Ocean and Earth Sciences, Xiamen University, Xiamen, China

<sup>3</sup>Fujian Engineering Research Center for Ocean Remote Sensing Big Data, Xiamen University, Xiamen, China

**Correspondence:** Kévin Robache (kevin.robache@univ-littoral.fr) and François G. Schmitt (francois.schmitt@cnrs.fr)

**Abstract.** In this study the multi-scale dynamics of 38 oceanic and atmospheric  $p\text{CO}_2$  time series from fixed Eulerian buoys recorded with three-hour resolution are considered. The difference between these time series, the sea surface temperature and the sea surface salinity data were also studied. These series possess multi-scale turbulent-like fluctuations and display scaling properties from three hours to the annual scale. Scaling exponents are estimated through Fourier analysis and their average quantities considered globally for all parameters, as well as for different ecosystems (e.g. coastal shelf, coral reefs, open ocean). Sea surface temperature is the only parameter for which a spectral slope close to  $5/3$  is found, corresponding to a passive scalar in homogeneous and isotropic turbulence. The other parameters had smaller spectral slopes, from 1.18 to 1.35. By using empirical mode decomposition of the time series, together with generalized Hilbert spectral analysis, the intermittency of the time series was considered in the multifractal framework. Concave moment functions were estimated and Hurst index and intermittency parameters estimated in the framework of a lognormal multifractal fit. It is the first time that atmospheric and oceanic  $p\text{CO}_2$  and their difference  $\Delta p\text{CO}_2$  are studied using such intermittent turbulence framework. The  $\Delta p\text{CO}_2$  time series was shown to possess power-law scaling with an exponent of  $\beta = 1.32 \pm 0.2$ .

## 1 Introduction: turbulent carbon dioxide fluxes at the air-sea interface

Anthropogenic global  $\text{CO}_2$  emissions have been rising since the last century (Pathak et al., 2022; Liu et al., 2022), increasing from around  $4.6 \pm 0.7 \text{ GtC y}^{-1}$  in the 1960s to around  $11.1 \pm 0.9 \text{ GtC y}^{-1}$  in recent years (Friedlingstein et al., 2023), and are linked with climate change (Anderson et al., 2016; Alola and Kirikkaleli, 2021). These emissions are mitigated by different mechanisms at different scales, from climate to small scale turbulence. This is especially true in the oceans, which absorbs around 25 % of annual anthropogenic emissions (Friedlingstein et al., 2023). It is known that several other mechanisms influence the  $\text{CO}_2$  dynamics in the ocean and the atmosphere at different spatial and temporal scales. For example, terrestrial biology (Keenan et al., 2012; Crisp et al., 2022), land chemistry (Roland et al., 2013), volcanism and human activities (Yue and Gao, 2018) can lead to variations of atmospheric  $\text{CO}_2$ . Furthermore, the ocean plays a major role in the carbon cycle through its interactions with the atmosphere and can absorb or release  $\text{CO}_2$  via physical and biological pumps (De La Rocha and



Passow, 2014; Yamamoto et al., 2018). These pumps are composed of numerous oceanic processes which also enable carbon sequestration at different timescales in the water column, e.g. through phytoplankton blooms and the thermo-haline circulation (Falkowski et al., 2000; De La Rocha and Passow, 2014) and in the sediment (Henson et al., 2019).

Globally, at large temporal and spatial scales, the ocean is a sink of carbon dioxide. However, locally in time and space, the ocean may be a sink or a source of carbon dioxide. In order to understand this better, *in-situ* observations are necessary. Here we consider high-frequency fixed points data at different parts of the global ocean, and focus on the influence of turbulence on their flux. The air-sea carbon dioxide flux is usually written as (Wanninkhof, 2014):

$$F_{\text{CO}_2} = k(U) \cdot K_0 \cdot \Delta p\text{CO}_2 \quad (1)$$

where  $K_0$  is the solubility ( $\text{mol L}^{-1} \text{atm}^{-1}$ ),  $k(U)$  is the gas transfer velocity ( $\text{cm h}^{-1}$ ) which depends on the surface wind speed  $U$ , and  $\Delta p\text{CO}_2 = p\text{CO}_{2 \text{ sw}} - p\text{CO}_{2 \text{ air}}$  is the difference between partial pressures of carbon dioxide in equilibrium with surface water and in the air above the seawater. Turbulence has a direct influence on the different components of this formula:  $K_0$  depends on temperature and salinity, which are turbulent scalars,  $k$  depends on wind turbulence on the atmospheric surface, and  $\Delta p\text{CO}_2$  depends on two scalars both advected by turbulence. Since  $k$  and  $K_0$  are both positive parameters, the direction of the flux is determined in the difference  $\Delta p\text{CO}_2$ : when  $\Delta p\text{CO}_2 > 0$ , the flux goes from the sea to the atmosphere, and when  $\Delta p\text{CO}_2 < 0$  the ocean is locally a sink of carbon dioxide. In this work we focus on the scaling properties of atmospheric and oceanic carbon dioxide partial pressure and on their difference, using a database of Eulerian time series recorded at a time resolution of 3 hours. This is considered as high-frequency measurement, compared to lower-frequency measurements done from e.g. weekly or monthly sampling. In oceanography, previous work from temperature Eulerian sampling (Derot et al., 2016) on pH and carbonate dynamics (Schmitt et al., 2008; Zongo and Schmitt, 2011), as well as works in atmospheric turbulence in the boundary-layer (Schmitt et al., 1994; Katul et al., 1995; Schmitt, 2007; Calif and Schmitt, 2012, 2014) have shown that turbulent fluctuations at fixed points can be detected from hourly scales to a large scale of about 3 months. The present data set is therefore analyzed here using methods from the field of turbulence in order to consider their scaling properties.

In the following section, the database chosen in this work is presented in section 2. Then the power spectral exponents are given and their averaged values are discussed in section 3. Section 4 presents intermittency analysis and the discussion and conclusion of this work are in section 5.

## 2 Presentation of the database

In this work, a published *in situ* observational database provided by Sutton et al. (2019) is analyzed. It contains observations from 40 fixed-point autonomous buoys distributed in the Pacific, Indian, Southern and Atlantic oceans. Two sites were discarded due to different sampling frequencies, and we have considered here 38 time series, whose locations are illustrated in Fig. 1 and are listed in the Appendix. For each buoy, the following parameters are recorded every 3 hours: sea surface temperature (SST), sea surface salinity (SSS), seawater partial pressure of  $\text{CO}_2$  ( $p\text{CO}_{2 \text{ sw}}$ ) and atmospheric partial pressure of  $\text{CO}_2$  ( $p\text{CO}_{2 \text{ air}}$ ). SST and SSS are measured using a multiparameter sonde (Sea-Bird Electronics 16plus V2 SeaCAT or a SBE 37 MicroCAT

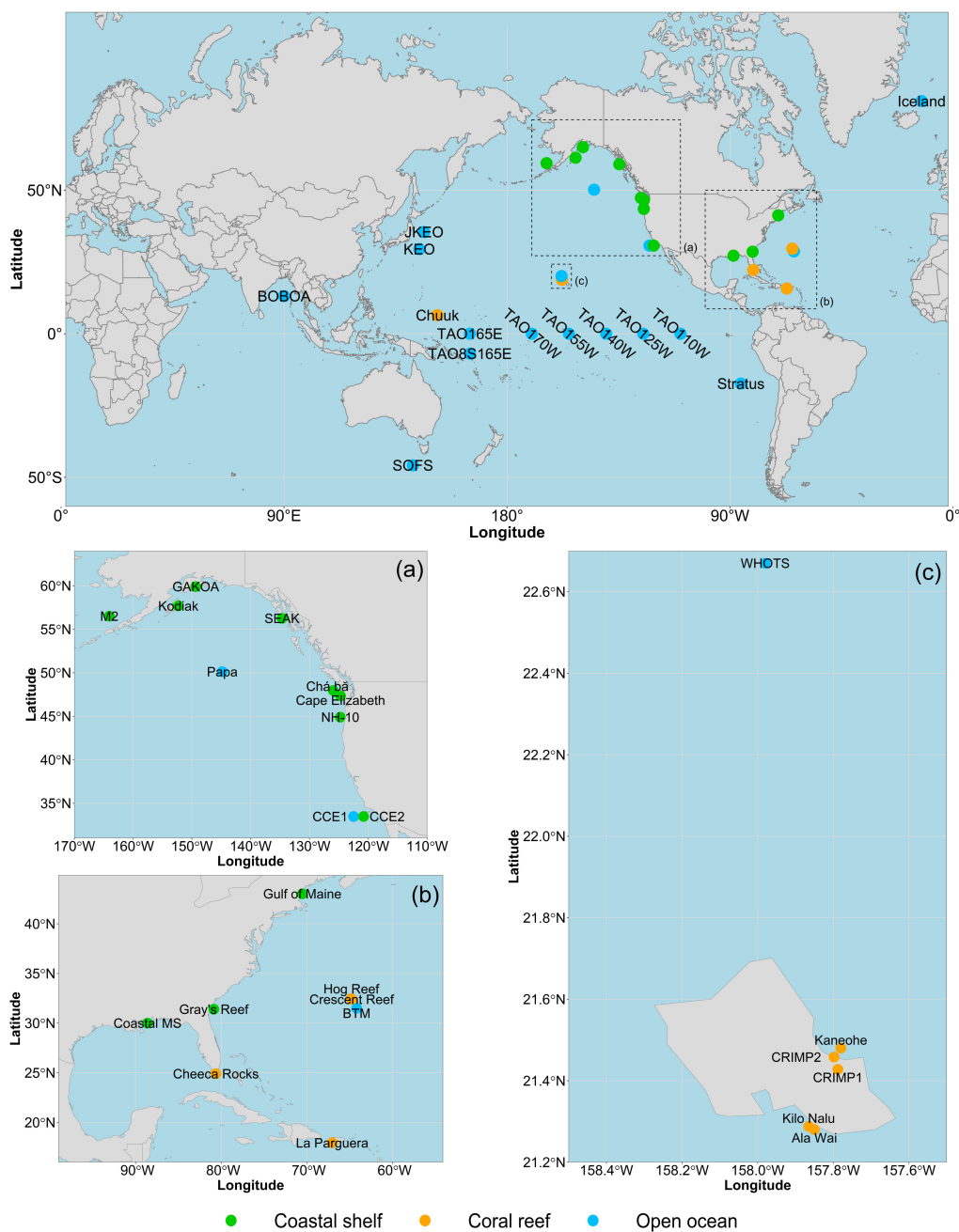


**Figure 1.** Maps of the position of 38 fixed position observation time series adapted from Sutton et al. (2019) with the same classification corresponding to a color code for coastal shelf buoys, coral reefs, and open ocean ecosystems.

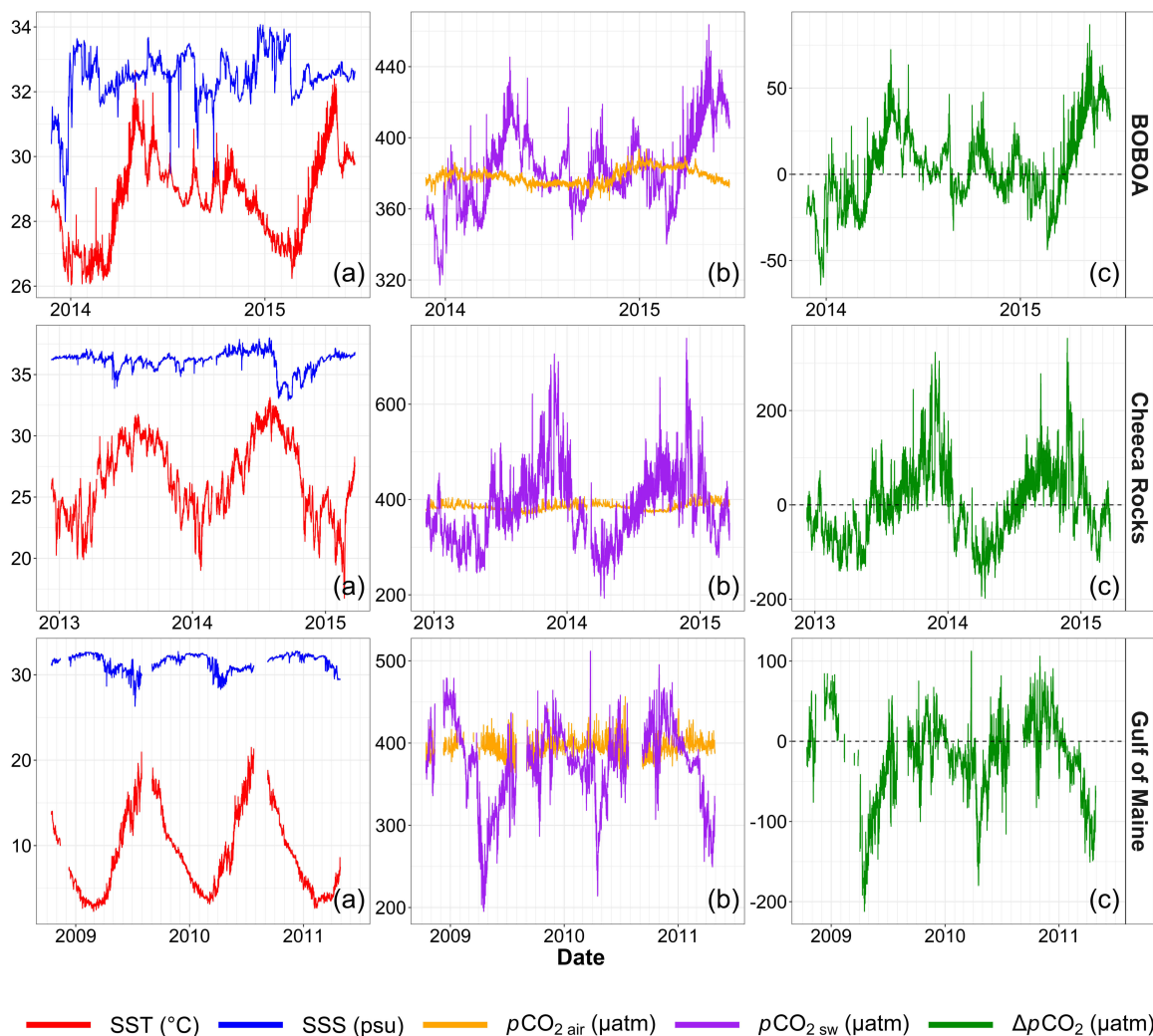


**Figure 2.** Portions of time series from the BOBOA (Bay of Bengal, Indian Ocean), Cheeca Rocks (Caribbean, North Atlantic Ocean) and Gulf of Maine (North Atlantic Ocean) buoys: (a) the sea surface temperature and salinity, (b) the atmospheric and oceanic  $p\text{CO}_2$ , and (c) their difference.

55 depending on the site) in the upper layer at a depth of about 0.5 m. The  $p\text{CO}_2$  time series are calculated from the molar fraction  $x\text{CO}_2$  by the MAPCO<sub>2</sub> sensor, which is an optical sensor measuring the infrared absorption by the air in comparison with the infrared absorption of a reference gas. Atmospheric measures are done between 0.5 and 1 m from the sea surface (Sutton et al., 2014, 2019).

These buoys are classified by the authors in three categories based on the type of ecosystem in which the buoy is located.  
 60 In the present work, different properties according to these ecosystems are considered. Among the 38 series, there are 11



series belonging to the coastal shelf, 10 series belonging to coral reefs, and 17 series belonging to the open ocean. The data paper presenting the database has highlighted the appearance of anthropogenic trends and seasonality (Sutton et al., 2019). The database has also been used in other works: Torres et al. (2021) were interested in the mean and extreme diurnal variability of these series and have highlighted their spatial and temporal properties. These data were also used for  $p\text{CO}_2$  data modelling purposes (Chau et al., 2022; Kwiatkowski et al., 2023).

As an example, data from 3 sites, one from each ecosystem type, are shown in Fig. 2. They correspond to the BOBOA (Bay of Bengal, open ocean), Cheeca Rocks (Gulf of Mexico, coral reefs) and Gulf of Maine (North Atlantic Ocean, coastal shelf) time series and illustrate the multiscale variability of all the studied parameters. It is also visible in this figure that for all cases the time series of  $p\text{CO}_2_{\text{air}}$  presents less relative fluctuations than  $p\text{CO}_2_{\text{sw}}$ . In order to consider this property for all series, the mean, the standard deviation, and the variation coefficient (ratio of the standard deviation to the mean value) of atmospheric and oceanic carbon dioxide partial pressures are estimated for all buoys. These quantities averaged for the three buoy categories are reported in Table 1. It shows that  $p\text{CO}_2_{\text{air}}$  presents much less relative fluctuations than  $p\text{CO}_2_{\text{sw}}$ : the mean values are of the same order of magnitude whereas the variation coefficients are 6 to 8 times lower. For  $p\text{CO}_2_{\text{air}}$  it is between 2 and 3 % and for  $p\text{CO}_2_{\text{sw}}$  it is between 13 and 25 %. Globally, the variation coefficient for coastal shelves is larger for atmospheric series and much larger for oceanic time series. For coral reefs and open-ocean ecosystems, the mean and standard deviations are similar.

This property can be explained by the better mixing of the atmosphere (Sarmiento and Gruber, 2002). Indeed, the diffusivity coefficient of  $\text{CO}_2$  in the atmosphere ( $0.16 \text{ cm}^2 \text{ s}^{-1}$  at  $20.1 \text{ }^\circ\text{C}$ ; Pritchard and Currie, 1982) is about 10,000 times higher than in the seawater ( $1.6 \cdot 10^{-5} \text{ cm}^2 \text{ s}^{-1}$  at  $20 \text{ }^\circ\text{C}$ ; Emerson and Hamme, 2022).

**Table 1.** Statistical values based on all the raw  $p\text{CO}_2$  time series available in Sutton et al. (2019). The mean and standard deviation values are given in  $\mu\text{atm}$  and variation coefficient are given in %.

| Scalar                      | Site category | Mean $\pm \sigma$ ( $\mu\text{atm}$ ) | Variation coefficient (%) |
|-----------------------------|---------------|---------------------------------------|---------------------------|
| $p\text{CO}_2_{\text{air}}$ | Coastal shelf | $393 \pm 11$                          | 2.8                       |
|                             | Coral reefs   | $382 \pm 9$                           | 2.4                       |
|                             | Open ocean    | $379 \pm 9$                           | 2.4                       |
| $p\text{CO}_2_{\text{sw}}$  | Coastal shelf | $348 \pm 85$                          | 24.4                      |
|                             | Coral reefs   | $407 \pm 53$                          | 13                        |
|                             | Open ocean    | $406 \pm 55$                          | 13.5                      |

Next, the difference  $\Delta p\text{CO}_2$  is considered. First, the conditional means and standard deviations of positive and negative values are estimated, averaged over each site of each category, and shown in Table 2. The order of magnitude of the conditional mean for positive values is of the same order for the three categories, while large variations (a ratio greater than 4) are found for the conditional average of negative values. For coral reefs and open ocean ecosystems, the overall average of positive values is much larger (almost double) than the average of negative values (in amplitude). For coastal shelf ecosystems, this proportion is reversed, and the conditional average of positive values is much smaller in amplitude than the conditional average of negative



**Table 2.** Conditional means, standard deviations and average proportions of positive and negative values of all the  $\delta = \Delta p\text{CO}_2$  ( $\mu\text{atm}$ ) time series averaged for each buoy site category. Conditional averages are first estimated for each time series. Then the mean and standard deviations indicated in the table are estimated from these mean values.

| Site category | Mean $\pm \sigma$ ( $\mu\text{atm}$ ) |  | Average proportion (%) |                   |
|---------------|---------------------------------------|--|------------------------|-------------------|
|               | $\langle \delta   \delta > 0 \rangle$ | $-\langle \delta   \delta < 0 \rangle$ | $\%_{\delta > 0}$      | $\%_{\delta < 0}$ |
| Coastal shelf | $50 \pm 37$                           | $92 \pm 32$                            | 24.7                   | 75.3              |
| Coral reefs   | $52 \pm 26$                           | $26 \pm 19$                            | 70.0                   | 30.0              |
| Open ocean    | $49 \pm 42$                           | $22 \pm 18$                            | 55.1                   | 44.9              |

85 values. These numbers do not directly reflect the sink or source of carbon dioxide of the different ecosystems, since it also depends on the proportion of time in the negative or positive values. It indicates that when it is a sink, globally the coastal shelf ecosystems are more active sinks compared to coral reefs or open ocean ecosystems. Concerning the proportion of negative and positive values shown in the same table, it is seen that the coastal shelf sites are much more often sinks than source (70 % versus 30 %), a proportion that is reversed for the coral reef sites. In the open ocean, there is a slight proportion in favor of  
 90 sinks.

The probability density functions (PDF) of  $\Delta p\text{CO}_2$  are also presented in Fig. 3 on a log scale. In these figures, the time series of  $\Delta p\text{CO}_2$  are centered (subtraction of the mean and division by the standard deviation) and then considered globally for each ecosystem (coral reefs, open ocean, coastal shelf). A Gaussian PDF is also shown for comparison. These figures show that the difference  $\Delta p\text{CO}_2$  is non-Gaussian, except for the negative values of the coastal shelf buoys. In all cases there are  
 95 more large positive values than in the Gaussian law. For open ocean buoys the PDF is symmetric whereas for the two other categories it is asymmetric, with more large positive values than negative ones.

### 3 Fourier spectral analysis

Fourier spectral analysis was applied to all series. Some portions of these time series have a time step shorter than 3 hours: in order to have homogeneous time steps, these portions have been averaged to have a regular sampling of 3 hours. As shown  
 100 in Fig. 2, there are also large portions of missing values due to failures in measuring devices or maintenance operations. In such a case, no interpolation or averaging is performed and the following method is used. First, the autocorrelation function is estimated, which by definition can be considered only for existing data and can deal with missing values:  $C(\tau) = \langle X(t)X(t + \tau) \rangle$  where  $X$  is a stationary time series with zero mean and  $\tau$  is a time increment. Then the Wiener-Khinchine theorem is used to consider the power spectrum as the Fourier transform of the autocorrelation function:

$$105 \quad E(f) = \int_{-\infty}^{+\infty} C(\tau) \exp(-2i\pi\tau f) d\tau \quad (2)$$

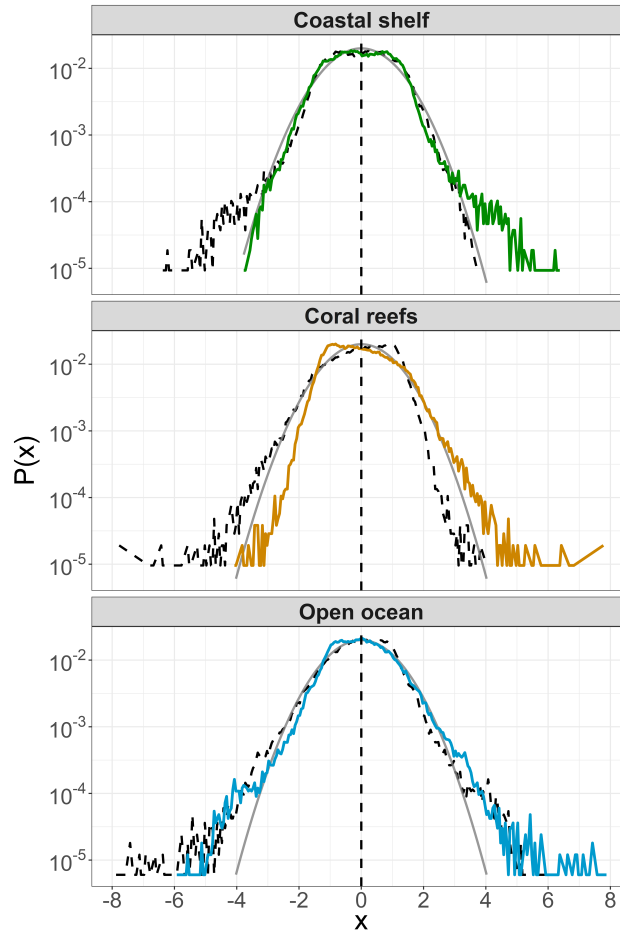


**Figure 3.** Probability density function (PDF) of centered time series of  $\Delta p\text{CO}_2$  considered for each site category. The black dotted lines are the symmetric PDFs and the grey continuous lines are the Gaussian PDFs. The density has been calculated using a band with of 0.05. The value represented for the x-axis is the middle value of each range.

where  $f$  is the frequency and  $E(f)$  the Fourier spectral density. Since time series are considered within the framework of turbulence forcing, scaling regimes are expected with the following power-law relation (Gao et al., 2021):

$$E(f) \sim f^{-\beta} \quad (3)$$

where “ $\sim$ ” means proportionality and  $\beta > 0$  is the spectral slope. Let us recall that in homogeneous and isotropic turbulence, the famous Kolmogorov 1941 (K41) relation corresponds to a scaling law for the velocity field with a value of  $\beta = 5/3$  (Kolmogorov, 1941). In such a framework, passive scalars advected by the turbulent velocity are also scaling with a scaling slope value of  $\beta = 5/3$  (Obukhov, 1949; Corrsin, 1951). In the ocean, temperature and salinity are generally considered to be passive scalars advected by the turbulent velocity field; whereas other scalars can also be studied, such as dissolved oxygen,



115 concentrations in nutrients, pH and the concentration or partial pressure of carbon dioxide. Other values of the spectral slope  
 have been reported and can be interpreted as the signature of a chemical or biological activity (Seuront et al., 1996; Schmitt  
 et al., 2008; Zongo and Schmitt, 2011).

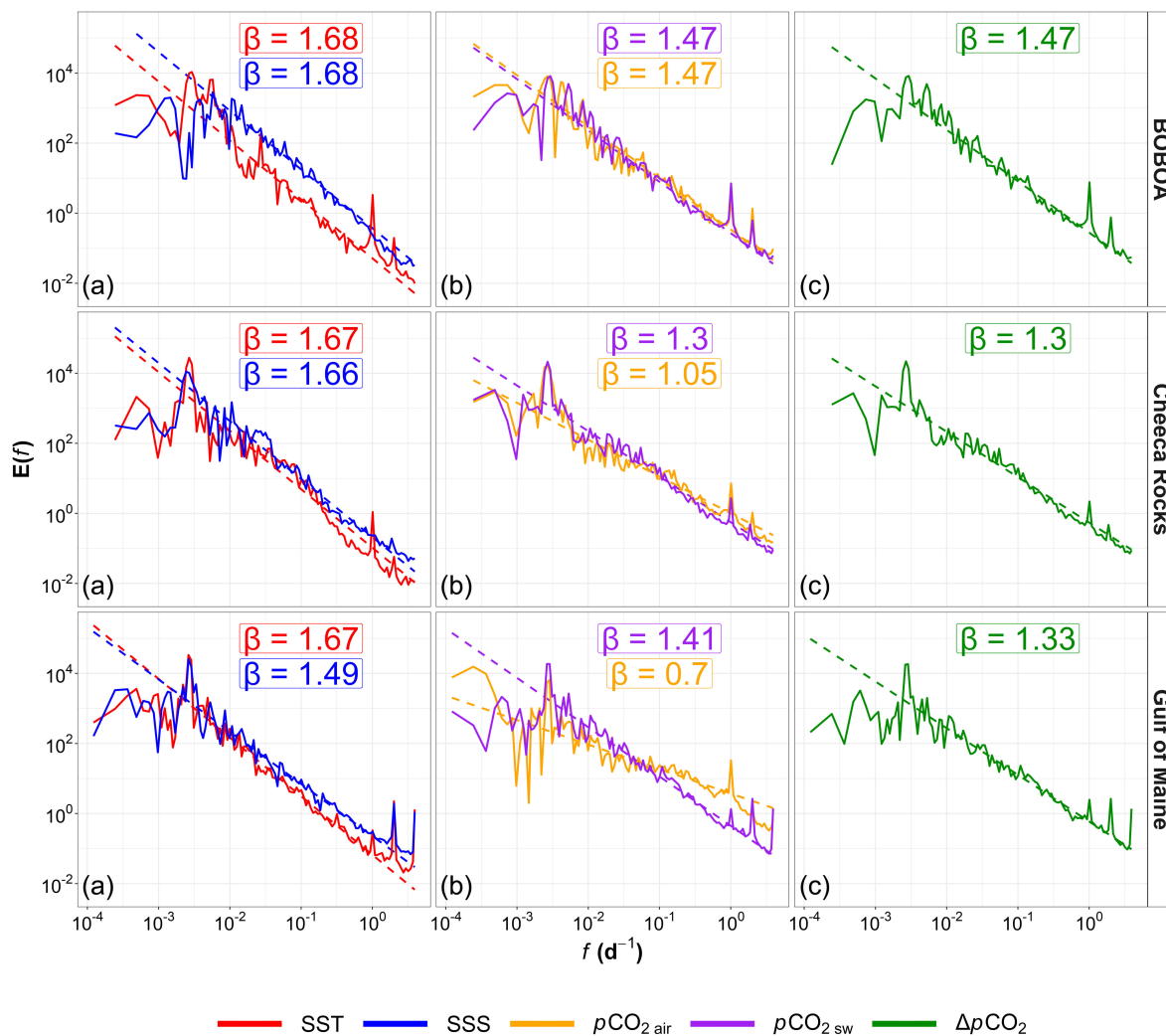


**Figure 4.** Fourier spectra represented in log-log for data from BOBOA (Bay of Bengal, Indian Ocean), Cheeca Rocks (Caribbean, North Atlantic Ocean) and Gulf of Maine (North Atlantic Ocean) buoys (see Fig. 2). The dotted lines represent the power-law fits and the slopes are given in each figure for (a) SST and SSS, (b) atmospheric and oceanic  $pCO_2$  and (c) their difference.





### 3.1 Mean values of spectral slopes

Raw Fourier spectra can be quite noisy, preventing clear detection of scaling ranges. To prevent this, each spectrum is averaged by decade; this does not destroy spectral pikes, but suppresses random fluctuations and provides smoother spectra. Over scaling ranges detected visually, the precise value of the spectral slope is estimated by using a least squares linear fit applied to the logarithmic values. To illustrate the scaling power spectra, the Fourier spectral plots are displayed for the three time series in Fig. 4, chosen as representative of each ecosystem: BOBOA (Bay of Bengal, open ocean), Cheeca Rocks (Gulf of Mexico, coral reefs) and Gulf of Maine (North Atlantic Ocean, coastal shelf). In each case, the scaling is found from the smallest scale (3 hours to a large scale of 1 year). Pikes are found in many cases for the annual cycle, and also for the daily and 12 hour time scales, the latter corresponding to the tidal influence. The amplitude of the pikes is not the same for each series. In some cases (i.e. salinity), the scaling at high frequency is not found below the daily time scale.

As shown in these figures, the values of the spectral slopes are variable in the range of 0.7 to 1.68 depending on the time series. This is performed for all  $38 \times 5$  series: a spectral slope is extracted in each case, and finally the mean and standard deviations estimated over series of both ecosystems are given in Table 3. It is found that the SST is the scalar with the lowest standard deviation in spectral slopes. The averaged SST spectral slope is also close to the value  $5/3$ , the theoretical value expected in the case of homogeneous and isotropic turbulence. Only in few cases the SST spectral slopes is much smaller than  $5/3$ : for M2, Coastal MS, Kaneohe. Different explanations can be given for this. First, M2 is an Alaskan buoy where ice is seasonal (Jin et al., 2007; Stabeno et al., 2010). This phenomenon could be the origin of a peculiar scaling. Second, Coastal MS is a buoy located in the Mississippi Delta. Rivers can influence the physicochemical parameters of coastal waters, such as temperature, salinity (Crossland et al., 2005; Walker et al., 2005) and also  $p\text{CO}_2$  (Kealoha et al., 2020). Thirdly, Kaneohe is situated in Kaneohe Bay (Hawaii). In this region, the Kaneohe stream and other streams have an impact on the marine environment (Drupp et al., 2011), which could influence the spectral slope of the temperature field. The mean spectral slopes for the other scalars are less than  $5/3$ . The mean values for SSS, seawater  $p\text{CO}_2$  and  $\Delta p\text{CO}_2$  are close to each other. For the atmospheric  $p\text{CO}_2$ , the averaged spectral slope is the lowest. These differences in spectral slopes could be due to biological or chemical activity.

**Table 3.** Mean and standard deviations of spectral slopes for all 5 parameters, estimated for the 38 global time series.

| Scalar                      | Mean $\pm \sigma$ |
|-----------------------------|-------------------|
| SST                         | $1.61 \pm 0.17$   |
| SSS                         | $1.35 \pm 0.29$   |
| $p\text{CO}_2_{\text{air}}$ | $1.18 \pm 0.31$   |
| $p\text{CO}_2_{\text{sw}}$  | $1.34 \pm 0.22$   |
| $\Delta p\text{CO}_2$       | $1.32 \pm 0.20$   |

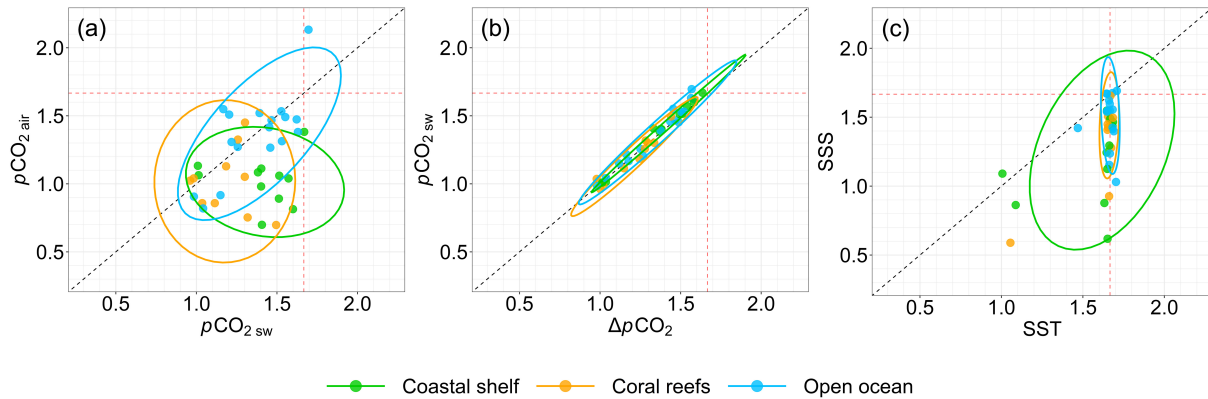


**Figure 5.** Scatter-plots of the Fourier spectral slopes, each dot corresponding to a given time series, and its color corresponding to the ecosystem site: (a) atmospheric versus sea water  $p\text{CO}_2$ ; (b) sea water  $p\text{CO}_2$  versus the difference  $\Delta p\text{CO}_2$  and also (c) SSS versus SST. The ellipses are calculated for each ecosystem from a 95 % confidence interval of the multivariate  $t$ -distribution. The vertical and horizontal red dotted lines represent the value  $5/3$ . The black dotted line represents the first bisector  $y = x$ .

The scaling properties of atmospheric  $\text{CO}_2$  have been reported in previous work. Spectral slopes close to  $5/3$  have been found at high frequencies (typically for scales smaller than a few seconds, from 0.2 to 10 or 25 Hz) for measurements in the atmospheric boundary layer over a forest (Anderson et al., 1986), over vegetated fields (Ohtaki, 1985; Gao et al., 2020), over the ocean (Ohtaki et al., 1989), or over a littoral area (Sahlée et al., 2008). A more recent study reported measurements of atmospheric  $\text{CO}_2$  using a tower 5 meters above the ground in a continental zone. Scaling properties were found for scales of 10 seconds to 15 minutes, with a scaling slope of  $\beta = 1.2$  (Gao et al., 2020). This value is closer to the mean value found here for this parameter. However, the scales considered in the present study are much larger than the ones used in these works and cannot be directly compared.

Figure 5 represents scatter plots of the spectral slope of some parameters. The first subfigure (Fig. 5a) shows that there is no direct link between the spectral slopes of the atmospheric and oceanic  $p\text{CO}_2$ ; the central figure (Fig. 5b) demonstrates that there is a direct link between the spectral slope of the marine measurements and of the difference  $\Delta p\text{CO}_2$ : this comes from the fact that, as seen above, the atmospheric measurements display much less relative fluctuations, so that the oceanic fluctuations dominate in the difference  $\Delta p\text{CO}_2$ . This dominance is reflected in the spectral slopes. The last plot (Fig. 5c) shows that the temperature values are very close to the theoretical value of  $5/3$  obtained for homogeneous and isotropic turbulence, while SSS, which is also often assumed to be a turbulent passive scalar (Thorpe, 2005, 2007) displays scaling properties but with spectral slopes which are not compatible with a turbulent passive scalar.

### 3.2 Analysis of spectral slopes for each ecosystem

Here statistical analysis is done over the spectral slopes of time series belonging to different ecosystems (coastal areas, coral reefs and open ocean). The different spectral slopes for all 3 ecosystems are represented as boxplots in Fig. 6; the mean values

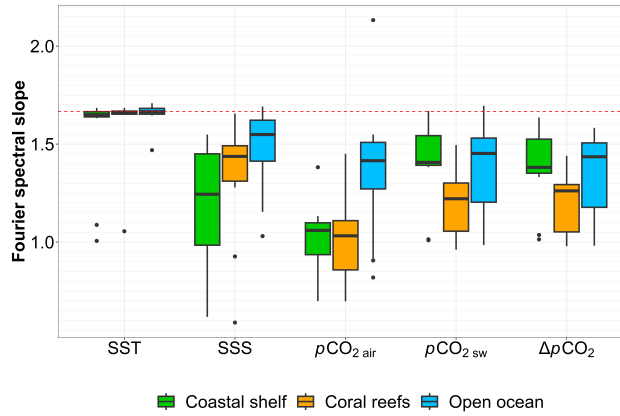


**Figure 6.** Representation using boxplots of all Fourier spectral slopes according to the site ecosystem (coastal shelf; coral reefs and open ocean). The horizontal dashed line corresponds to the theoretical value of  $5/3$  expected for passive scalars in homogeneous and isotropic turbulence.

160 are also given in Table 4. Concerning SSS, for the coastal shelf sites, there is greater variability for the spectral slopes. The departure from the passive scalar values is smaller for open-ocean sites. In coastal areas, the departures from a passive scalar slope could be due to coastal forcing induced by river flows associated with shallow depths (Crossland et al., 2005). Some sites in the Equatorial Pacific (coral reefs ecosystem) have slopes very different from  $5/3$ , which could be due to the associated rainfall in these areas (Turk et al., 2010). For  $p\text{CO}_2_{\text{air}}$  the values for coral reefs and coastal shelf ecosystems seem similar, while for the open ocean steeper slopes are found. As mentioned above for global values, for each ecosystem, the spectral slopes for the difference  $\Delta p\text{CO}_2$  are very similar to those for  $p\text{CO}_2_{\text{sw}}$ . Regarding the latter, it is visible that the spectral slopes are less steep for coral reef sites: such a strong departure from a passive scalar could be the effect of strong biological activity in coral reefs. The ellipses shown in Fig. 5 are calculated for each ecosystem from a 95 % confidence interval of the multivariate  $t$ -distribution. They do not differentiate the ecosystems in Figs. 5a,b. Only in Fig. 5c, the ellipse computed for the coastal shelf sites is clearly different from the others, an indicator of greater variability in both the SSS and SST spectral slopes.

**Table 4.** Means and standard deviations based on extracted Fourier spectral slopes  $\beta$  for each studied scalar and for each ecosystem.

| Scalar                      | Coastal shelf   | Coral reefs     | Open ocean      |
|-----------------------------|-----------------|-----------------|-----------------|
| SST                         | $1.55 \pm 0.25$ | $1.6 \pm 0.19$  | $1.66 \pm 0.05$ |
| SSS                         | $1.19 \pm 0.3$  | $1.32 \pm 0.32$ | $1.48 \pm 0.19$ |
| $p\text{CO}_2_{\text{air}}$ | $1.02 \pm 0.18$ | $1.02 \pm 0.24$ | $1.37 \pm 0.3$  |
| $p\text{CO}_2_{\text{sw}}$  | $1.41 \pm 0.22$ | $1.2 \pm 0.17$  | $1.37 \pm 0.22$ |
| $\Delta p\text{CO}_2$       | $1.39 \pm 0.2$  | $1.2 \pm 0.16$  | $1.35 \pm 0.2$  |

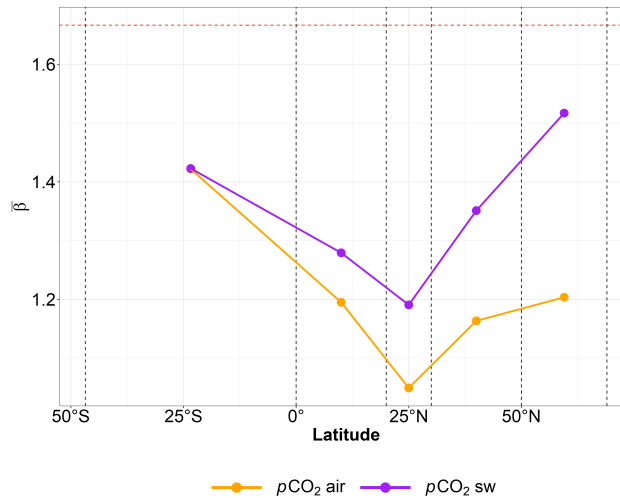


**Figure 7.** Average Fourier spectral slope  $\beta$  in function of the latitude. The red dotted line represent the value  $5/3$ . The ranges of values used for each point are represented by the black dotted lines:  $[46.8^\circ\text{S}; 0^\circ[$  (3 stations),  $[0^\circ; 20^\circ\text{N}[$  (9 stations),  $[20^\circ\text{N}; 30^\circ\text{N}[$  (7 stations),  $[30^\circ\text{N}; 50^\circ\text{N}[$  (13 stations) and  $[50^\circ\text{N}; 69^\circ\text{N}[$  (6 stations).

### 3.3 Latitudinal variability of $p\text{CO}_2$ spectral slopes

The spatial variation of the spectral exponents of  $p\text{CO}_2$  are considered in this section, for all series, regardless of the ecosystem to which they belong. Different bins of unequal length are chosen to perform averages, with approximately the same number of series in each bin. The result is shown in Fig. 7 where the limits of the bins are shown as dotted lines, and the mean values for atmospheric and oceanic partial pressures in carbon dioxide are displayed. The pattern is similar for both curves, with a minimal slope for tropical values (latitude around 20-30 degrees) in the northern hemisphere and an increase of the spectral slope as one moves away from this position. This latitudinal gradient can also be explained by the fact that there are more buy series belonging to the coral reef ecosystem in the database.

## 4 Multifractal intermittency

### 4.1 Extraction of intermittency exponents for a time series with periodicities

Turbulent time series are intermittent and possess large fluctuations on many different scales. Such fluctuations are classically studied by considering structure functions of the form  $\Delta X_\tau = X(t + \tau) - X(t)$ , corresponding to time increments at scale  $\tau$ . The scaling intermittent properties are considered by estimating the moments of order  $q$  of the structure functions (Frisch, 1995; Schmitt and Huang, 2016):

$$\langle |\Delta X_\tau|^q \rangle \sim \tau^{\zeta(q)} \quad (4)$$



where  $q > 0$  is the moment order (which can be non-integer) and  $\zeta(q)$  is the scaling exponent of the corresponding moment function. Larger moments correspond to more intense fluctuations and the whole  $\zeta(q)$  curve characterizes the multi-scale intermittency of the time series. The Fourier spectrum corresponds to a moment of order 2: the spectral exponent  $\beta$  is related with  $\zeta(2)$ :  $\beta = 1 + \zeta(2)$ .

190 Unfortunately, the periodicity in the series, even weak, is known to destroy the scaling properties of structure functions (Huang et al., 2011; Schmitt and Huang, 2016) and in this case other methods are needed to extract the scaling exponent  $\zeta(q)$ . This is done here in the spectral space, by using the Hilbert spectral analysis (HSA) associated with empirical mode decomposition (EMD), using the generalized HSA method. This method uses first the EMD, which is an algorithm developed to decompose the original time series into  $N$  other time series called intrinsic mode functions (IMFs; Huang et al.,  
 195 1998, 1999; Flandrin et al., 2004). This signal analysis has already been used to study multi-scale variability of  $\text{CO}_2$  time series (Landschützer et al., 2016; Zhang et al., 2022). The sum of IMFs  $C_i(t)$  and a residue  $r_n(t)$  give the original signal  $X(t)$ :

$$X(t) = \sum_{i=1}^N C_i(t) + r_n(t) \quad (5)$$

Missing values are first linearly interpolated to compensate for the fact that the EMD method requires a complete signal.  
 200 This iterative algorithm is based on a spline interpolation of local minima and maxima. Each IMF is a zero-mean time series localized in the frequency space. Their Hilbert transform is denoted  $\tilde{C}_i(t)$ :

$$\tilde{C}_i(t) = \frac{1}{\pi} \int_{-\infty}^{+\infty} \frac{C_i(\tau)}{t - \tau} d\tau \quad (6)$$

The analytic signal  $z_i = C_i + j\tilde{C}_i$  is a complex number that can be written as  $z_i = A_i(t)e^{j\theta_i(t)}$ , where  $A_i(t)$  is the local amplitude and  $\theta_i(t)$  the local phase of  $C_i(t)$ . Leaving the residual, the original signal can be rewritten as the sum of the real  
 205 part of all the analytic signals  $z_i$  as  $X(t) = \text{Re} \sum_{i=1}^N A_i(t)e^{j\theta_i(t)}$ . Here, a local instantaneous frequency is extracted from  $\omega = d\theta/dt$  (where the phase  $\theta(t)$  is given by  $\theta_i(t) = \tan^{-1} \tilde{C}_i(t)/C_i(t)$ ). A joint probability density function of frequency and amplitude  $p(\omega, A)$  is extracted from the data and a Hilbert power spectrum is computed as  $L_2(\omega) = \int_0^{+\infty} p(\omega, A)A^2 dA$ . This Hilbert spectrum is similar to the Fourier spectrum  $E(f)$  (Huang et al., 2008). To consider the intermittency of the signal in the EMD-HSA framework, the Hilbert marginal spectrum  $L_q(\omega)$  is calculated for different statistical moments  $q$  (Huang et al.,  
 210 2008, 2011; Schmitt and Huang, 2016) as  $L_q(\omega) = \int_0^{+\infty} p(\omega, A)A^q dA$ . For scaling time series, it has been shown that this can be written as:

$$L_q(\omega) \sim \omega^{-\xi(q)} \quad (7)$$

for frequencies belonging to the scaling range, where the scaling exponent in the amplitude-frequency space  $\xi(q)$  is related to the structure functions scaling exponents (also called scaling moment function) as  $\zeta(q) = \xi(q) - 1$ . It was previously shown  
 215 using simulations that this EMD-HSA approach, with the estimation of multifractal exponents in the frequency space, is not affected by the periodicity in the original series (Huang et al., 2011).



This method is applied here to the time series to extract intermittency exponents. There are several intermittency models published in the literature (Schmitt and Huang, 2016). The classical one is the lognormal model originally proposed by Kolmogorov (Kolmogorov, 1962). This model provides a quadratic expression which is chosen here as a fit of the nonlinear curve of the  $\zeta(q)$  function. In this framework the scaling exponent can be written as  $\zeta(q) = qH - K(q)$  where  $H = \zeta(1)$  is the Hurst exponent (usually  $0 \leq H \leq 1$ ) and  $K(q)$  captures the intermittency corrections. In the lognormal framework, only one more parameter is needed here, the intermittency parameters  $\mu = K(2) = 2H - \zeta(2)$ . These two parameters are extracted from the EMD-HSA exponents  $\xi(q)$ .

## 4.2 Intermittency analysis of the database

The EMD-HSA method has been applied here only to 28 stations among the 38 studied stations: for the remaining 10 stations (8 coral reefs and 2 open ocean sites) the scaling of moments of order larger than 2 was destroyed due to a too low number of data points in the series. The results for the 3 specific stations chosen as representative of the three ecosystems are shown in Fig. 8, for moments from 0 to 4. The shape of scaling exponent  $\zeta(q)$  is concave as expected. Some scaling exponents are almost linear, which means that the intermittency correction is weak. The overall nonlinear and concave shapes are captured by the two parameters  $H$  and  $\mu$ . The larger  $\mu$ , the more important the intermittency corrections are. These parameters are estimated for each series, and their mean and standard deviation are provided in Table 5. The values of  $H$  are estimated from the first-order moment using the EMD-HSA method, whereas the values of the spectral slopes  $\beta$  are estimated using Fourier analysis: this means that there may be some slight differences due to the method and intermittency corrections, but globally the relation  $\beta \simeq 1 + 2H$  is approximately valid.

Concerning the intermittency parameter, let us note that if the same procedure is applied to the velocity and passive scalar in fully developed hydrodynamic turbulence ( $H = \zeta(1)$  and  $\mu = 2\zeta(1) - \zeta(2)$ ), we obtain values of  $H = 0.37$  and  $\mu = 0.04$  for the velocity field (Schmitt, 2006) and  $H = 0.38$  and  $\mu = 0.12$  for the passive scalar field (Schmitt et al., 1996). The values found here for  $\mu$  are of the same order of magnitude, and sometimes slightly smaller than what is found for the passive scalar in hydrodynamic turbulence. The results obtained show also that overall, the intermittency parameter is greater for the salinity and atmospheric partial pressure of carbon dioxide. It also shows for the first time the multifractal intermittency of oceanic and atmospheric  $p\text{CO}_2$  fields.

## 5 Discussion and conclusion

Here a published database of high-frequency fixed point buoys recorded at 3 hours resolution has been considered. The dynamics of sea surface salinity, sea surface temperature, seawater and atmospheric partial pressure of carbon dioxide and the difference  $\Delta p\text{CO}_2$  have been considered for each site. These quantities are scalars forced and transported by turbulence; they display large turbulent-like fluctuations in many different scales and their dynamics have been considered on multiscale by estimating the scaling properties using Fourier transform. It was found that these series have scaling properties from the smallest scale (3 hours) to one year. Mean spectral slopes have been estimated: the SST possessed spectral slopes on average close to

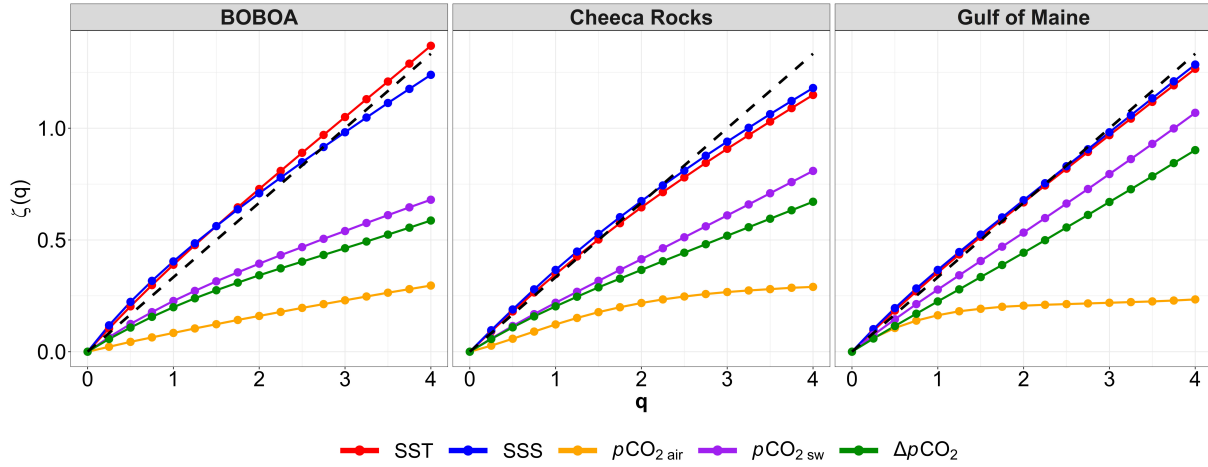


**Figure 8.** Scaling moment function  $\zeta(q) = \xi(q) - 1$  of the BOBOA, Cheeca Rocks and Gulf of Maine buoys time series for different statistical moments  $q$  from 0 to 4. The dashed line represents the theoretical relation  $q/3$  linked to a monofractal dynamics with  $H = 1/3$  as in homogeneous and isotropic turbulence with no intermittency.

**Table 5.** For all 5 parameters, the Hurst index  $H$  and the intermittency parameters  $\mu$ : mean and standard deviations estimated for the 28 time series.

| Scalar                      | $H$             | $\mu$           |
|-----------------------------|-----------------|-----------------|
| SST                         | $0.35 \pm 0.03$ | $0.03 \pm 0.03$ |
| SSS                         | $0.36 \pm 0.15$ | $0.08 \pm 0.07$ |
| $p\text{CO}_2_{\text{air}}$ | $0.22 \pm 0.17$ | $0.06 \pm 0.06$ |
| $p\text{CO}_2_{\text{sw}}$  | $0.27 \pm 0.07$ | $0.03 \pm 0.03$ |
| $\Delta p\text{CO}_2$       | $0.28 \pm 0.08$ | $0.03 \pm 0.03$ |

the value of  $5/3$  corresponding to 3D passive scalars in homogeneous and isotropic turbulence. The other scalars displayed values of the spectral slope  $\beta$  much smaller, from about 1.2 to 1.35. Such values have already been found for other scalars (fluorescence, pH) in marine waters for the same range of scales (Seuront et al., 1996; Schmitt et al., 2008; Zongo and Schmitt, 2011). Mean values were also estimated in average for different ecosystems (coastal shelf, coral reefs and the open ocean) and some differences could be detected. There were also latitudinal variations in these slopes.

The Kolmogorov-Obukhov-Corrsing slope of  $5/3$  for passive scalars was obtained through dimensional analysis. Let us emphasize here that similar theoretical explanations for the slopes close to  $6/5$ ,  $4/3$  or  $5/2$  for the scalars considered are not presently available; in future works dimensional analysis could be explored in this framework.

Power spectra correspond to second-order moments and medium fluctuations. To study the intermittent and multifractal properties of the series, the EMD-HSA method was used, since the classical structure function approach cannot be used for



series possessing periodicity as is the case here, with daily and tidal forcing. This approach could not be used for all series  
260 since it needs rather large datasets. It was used for 28 series and the multifractal properties were characterized by considering a  
lognormal fit, with the estimation of the Hurst exponent  $H$  and the intermittency parameter  $\mu$ . This showed that in general, the  
different time series possess multifractal properties with various intensity of the intermittency exponent (the largest being found  
in SSS and atmospheric  $p\text{CO}_2$ ). We may note also that the approach used here is consistent with previous works involving  
singular spectra analysis and assumptions of multifractality for oceanic  $p\text{CO}_2$  data (Hernández-Carrasco et al., 2015, 2018).

265 Considering  $p\text{CO}_2$  series, one of the interesting points in the present time series is the fact that simultaneous measurements of  
atmospheric and oceanic  $p\text{CO}_2$  are estimated. It was found that the variation coefficient of atmospheric  $p\text{CO}_2$  (ratio of standard  
deviation to the mean) is much lower than for the marine waters with a ratio of 6 to 8. Furthermore, the difference  $\Delta p\text{CO}_2$   
was studied here and shown to be scaling and multifractal. This is clearly related to turbulent forcing. Since the direction of  
the flux and the fact that a given site is a sink or a source of  $\text{CO}_2$ , is given by the difference  $\Delta p\text{CO}_2$ , such turbulent forcing is  
270 an important point for future studies: (i) perform the same analysis at smaller scales using higher resolution measurements; (ii)  
see more precisely how the turbulent forcing influences the sign of the difference, and (iii) how the intermittency properties of  
these differences is related with the forcing and the climate of a given site. The influence of the ecosystem found here for some  
average values of the parameter  $\beta$  is a first step in this direction.

*Code and data availability.* Data are freely accessible in Sutton et al. (2019, <https://doi.org/10.5194/essd-11-421-2019>). The code for the  
275 Fourier spectral analyzes is published in Gao et al. (2021).

*Author contributions.* FGS directed the research and KR performed the code and the analysis. YH helped with the code development and  
the finalization of the results. KR wrote the first draft and all authors revised and edited the manuscript.

*Competing interests.* The authors declare that no competing interests are present.

*Acknowledgements.* The Région Haut-de-France and the ANR project  $\text{CO}_2\text{Coast}$  (P.I. Hubert Loisel, ANR-20-CE01-0021) are acknowl-  
280 edged for cofunding of the PhD thesis of KR.

## Appendix A: Summary of the database





**Table A1.** Summary table of all the time series in the database studied (Sutton et al., 2019). The time resolution for each of these time series is 3 hours.

| Station        | Lat    | Long     | Category      | Start date       | End date         | Size   | % of missing data |       |                            |                             |                       |
|----------------|--------|----------|---------------|------------------|------------------|--------|-------------------|-------|----------------------------|-----------------------------|-----------------------|
|                |        |          |               |                  |                  |        | SST               | SSS   | $p\text{CO}_2_{\text{sw}}$ | $p\text{CO}_2_{\text{air}}$ | $\Delta p\text{CO}_2$ |
| Cape Elizabeth | 47.353 | -124.731 | Coastal shelf | 23/06/2006 06:00 | 30/10/2015 00:00 | 27,327 | 33.29             | 34.54 | 35.27                      | 34.76                       | 35.42                 |
| CCE2           | 33.479 | -120.814 | Coastal shelf | 17/01/2010 18:00 | 28/04/2015 00:00 | 15,411 | 13.6              | 13.61 | 13.91                      | 14.05                       | 14.27                 |
| Chá bã         | 47.963 | -125.958 | Coastal shelf | 17/07/2010 12:00 | 09/12/2016 09:00 | 18,696 | 49.23             | 51.24 | 49.47                      | 49.56                       | 49.61                 |
| Coastal MS     | 30     | -88.6    | Coastal shelf | 12/05/2009 21:00 | 30/03/2015 15:00 | 17,183 | 70                | 70    | 70.08                      | 70.1                        | 70.13                 |
| GAKOA          | 59.91  | -149.35  | Coastal shelf | 19/05/2011 21:00 | 20/01/2017 21:00 | 16,585 | 25.63             | 25.63 | 25.72                      | 25.88                       | 25.9                  |
| Gray's Reef    | 31.4   | -80.87   | Coastal shelf | 18/07/2006 09:00 | 15/10/2015 12:00 | 27,010 | 30.55             | 34.03 | 39.8                       | 34.25                       | 39.82                 |
| Gulf of Maine  | 43.023 | -70.542  | Coastal shelf | 29/08/2007 03:00 | 03/11/2015 15:00 | 23,909 | 28.57             | 28.58 | 29.32                      | 33.31                       | 33.41                 |
| Kodiak         | 57.7   | -152.31  | Coastal shelf | 30/03/2013 00:00 | 18/04/2016 18:00 | 8,927  | 7.11              | 7.11  | 7.29                       | 7.36                        | 7.38                  |
| M2             | 56.51  | -164.04  | Coastal shelf | 06/05/2013 06:00 | 29/05/2016 21:00 | 8,958  | 58.26             | 58.26 | 58.57                      | 58.58                       | 58.77                 |
| NH-10          | 44.904 | -124.778 | Coastal shelf | 03/04/2014 09:00 | 28/09/2015 18:00 | 4,348  | 36.02             | 36.02 | 41.86                      | 36.32                       | 42.04                 |
| SEAK           | 56.26  | -134.67  | Coastal shelf | 29/03/2013 03:00 | 22/07/2014 06:00 | 3,842  | 22.93             | 22.93 | 23.48                      | 23.35                       | 23.61                 |
| Ala Wai        | 21.28  | -157.85  | Coral reefs   | 07/06/2008 00:00 | 28/07/2014 18:00 | 17,943 | 26.1              | 26.1  | 26.48                      | 26.39                       | 26.71                 |
| Cheeca Rocks   | 24.91  | -80.624  | Coral reefs   | 08/12/2011 21:00 | 03/05/2016 12:00 | 12,862 | 16.25             | 16.28 | 16.47                      | 16.54                       | 16.57                 |
| Chuuk          | 7.46   | 151.9    | Coral reefs   | 18/11/2011 12:00 | 28/11/2015 00:00 | 11,765 | 4.28              | 4.28  | 4.75                       | 4.75                        | 4.81                  |
| Crescent Reef  | 32.4   | -64.79   | Coral reefs   | 27/11/2010 03:00 | 07/07/2015 15:00 | 13,469 | 21.69             | 21.69 | 21.81                      | 21.82                       | 21.83                 |
| CRIMP1         | 21.428 | -157.788 | Coral reefs   | 01/12/2005 03:00 | 30/05/2008 21:00 | 7,295  | 26.1              | 26.18 | 26.66                      | 26.68                       | 26.81                 |
| CRIMP2         | 21.458 | -157.798 | Coral reefs   | 11/06/2008 00:00 | 11/03/2013 09:00 | 13,876 | 18.52             | 18.52 | 19.92                      | 18.67                       | 20.06                 |
| Hog Reef       | 32.46  | -64.83   | Coral reefs   | 05/12/2010 03:00 | 07/01/2015 09:00 | 11,955 | 40.61             | 40.61 | 40.69                      | 40.65                       | 40.7                  |
| Kaneohe        | 21.48  | -157.78  | Coral reefs   | 30/09/2011 03:00 | 10/10/2016 09:00 | 14,699 | 47.79             | 52.96 | 53.16                      | 53.13                       | 53.18                 |
| Kilo Nalu      | 21.288 | -157.865 | Coral reefs   | 07/06/2008 18:00 | 02/02/2017 18:00 | 25,297 | 59.57             | 59.57 | 59.62                      | 59.81                       | 59.83                 |
| La Parguera    | 17.954 | -67.051  | Coral reefs   | 16/01/2009 21:00 | 11/01/2017 12:00 | 23,334 | 20.73             | 20.75 | 21.67                      | 21.71                       | 21.74                 |
| BOBOA          | 15     | 90       | Open ocean    | 25/11/2013 15:00 | 09/01/2017 03:00 | 9,125  | 22.9              | 22.9  | 23.36                      | 23.2                        | 23.36                 |
| BTM            | 31.5   | -64.2    | Open ocean    | 22/10/2005 00:00 | 01/10/2007 12:00 | 5,677  | 11.82             | 11.87 | 12.7                       | 12.08                       | 12.74                 |
| CCE1           | 33.48  | -122.51  | Open ocean    | 11/11/2008 18:00 | 26/10/2014 03:00 | 17,396 | 45.52             | 45.52 | 45.96                      | 45.66                       | 45.97                 |
| Iceland        | 68     | -12.67   | Open ocean    | 17/08/2013 03:00 | 02/11/2014 12:00 | 3,540  | 30.23             | 30.23 | 30.59                      | 32.01                       | 32.01                 |
| JKEO           | 37.93  | 146.52   | Open ocean    | 20/02/2007 12:00 | 03/10/2007 18:00 | 1,803  | 0.06              | 34.83 | 49.08                      | 48.25                       | 49.25                 |
| KEO            | 32.28  | 144.58   | Open ocean    | 26/09/2007 21:00 | 12/08/2015 00:00 | 23,010 | 18.04             | 18.35 | 20.93                      | 18.57                       | 20.99                 |
| Papa           | 50.13  | -144.84  | Open ocean    | 09/06/2007 21:00 | 16/06/2015 15:00 | 23,431 | 20.59             | 22.37 | 23.31                      | 22.55                       | 23.34                 |
| SOFS           | -46.8  | 142      | Open ocean    | 25/11/2011 06:00 | 15/10/2013 00:00 | 5,519  | 31.89             | 31.89 | 33                         | 32.43                       | 33.34                 |
| Stratus        | -19.7  | -85.6    | Open ocean    | 19/10/2006 21:00 | 03/04/2015 03:00 | 24,699 | 15.84             | 15.86 | 22.83                      | 22.85                       | 22.88                 |
| TAO110W        | 0      | -110     | Open ocean    | 20/09/2009 06:00 | 03/06/2017 03:00 | 22,504 | 57.84             | 57.75 | 63.62                      | 60.57                       | 63.62                 |
| TAO125W        | 0      | -125     | Open ocean    | 16/03/2005 03:00 | 06/02/2017 03:00 | 34,761 | 45.55             | 49.45 | 55.98                      | 52.98                       | 55.98                 |
| TAO140W        | 0      | -140     | Open ocean    | 23/05/2004 06:00 | 22/03/2015 15:00 | 31,644 | 40.74             | 50.37 | 55.12                      | 41.63                       | 55.12                 |
| TAO155W        | 0      | -155     | Open ocean    | 14/01/2010 15:00 | 17/11/2014 18:00 | 14,146 | 48.13             | 73.19 | 74.27                      | 73.6                        | 74.27                 |
| TAO165E        | 0      | 165      | Open ocean    | 24/02/2010 00:00 | 03/02/2013 00:00 | 8,601  | 41.25             | 63.26 | 72.48                      | 69.7                        | 72.48                 |
| TAO170W        | 0      | -170     | Open ocean    | 05/07/2005 00:00 | 15/05/2012 21:00 | 20,056 | 35.51             | 35.51 | 41.79                      | 36.16                       | 41.82                 |
| TAO8S165E      | -8     | 165      | Open ocean    | 23/06/2009 03:00 | 15/11/2011 09:00 | 7,003  | 4.4               | 13.85 | 14.61                      | 14.29                       | 14.62                 |
| WHOTS          | 22.67  | -157.98  | Open ocean    | 20/12/2004 15:00 | 15/07/2015 00:00 | 30,868 | 29.29             | 28.13 | 30.72                      | 30.13                       | 30.84                 |

## References

Alola, A. A. and Kirikkaleli, D.: Global Evidence of Time-Frequency Dependency of Temperature and Environmental Quality from a Wavelet Coherence Approach, *Air Quality, Atmosphere & Health*, 14, 581–589, <https://doi.org/10.1007/s11869-020-00962-z>, 2021.



- 285 Anderson, D. E., Verma, S. B., Clement, R. J., Baldocchi, D. D., and Matt, D. R.: Turbulence Spectra of CO<sub>2</sub>, Water Vapor, Temperature and Velocity over a Deciduous Forest, *Agricultural and Forest Meteorology*, 38, 81–99, [https://doi.org/10.1016/0168-1923\(86\)90051-1](https://doi.org/10.1016/0168-1923(86)90051-1), 1986.
- Anderson, T. R., Hawkins, E., and Jones, P. D.: CO<sub>2</sub>, the Greenhouse Effect and Global Warming: From the Pioneering Work of Arrhenius and Callendar to Today's Earth System Models, *Endeavour*, 40, 178–187, <https://doi.org/10.1016/j.endeavour.2016.07.002>, 2016.
- 290 Calif, R. and Schmitt, F. G.: Modeling of Atmospheric Wind Speed Sequence Using a Lognormal Continuous Stochastic Equation, *Journal of Wind Engineering and Industrial Aerodynamics*, 109, 1–8, <https://doi.org/10.1016/j.jweia.2012.06.002>, 2012.
- Calif, R. and Schmitt, F. G.: Multiscaling and Joint Multiscaling Description of the Atmospheric Wind Speed and the Aggregate Power Output from a Wind Farm, *Nonlinear Processes in Geophysics*, 21, 379–392, <https://doi.org/10.5194/npg-21-379-2014>, 2014.
- Chau, T. T. T., Gehlen, M., and Chevallier, F.: A Seamless Ensemble-Based Reconstruction of Surface Ocean pCO<sub>2</sub> and Air–Sea CO<sub>2</sub> Fluxes over the Global Coastal and Open Oceans, *Biogeosciences*, 19, 1087–1109, <https://doi.org/10.5194/bg-19-1087-2022>, 2022.
- 295 Corrsin, S.: On the Spectrum of Isotropic Temperature Fluctuations in an Isotropic Turbulence, *Journal of Applied Physics*, 22, 469–473, 1951.
- Crisp, D., Dolman, H., Tanhua, T., McKinley, G. A., Hauck, J., Bastos, A., Sitch, S., Eggleston, S., and Aich, V.: How Well Do We Understand the Land–Ocean–Atmosphere Carbon Cycle?, *Reviews of Geophysics*, 60, e2021RG000736, <https://doi.org/10.1029/2021RG000736>, 2022.
- 300 Crossland, C. J., Baird, D., Ducrotoy, J.-P., Lindeboom, H., Buddemeier, R. W., Dennison, W. C., Maxwell, B. A., Smith, S. V., and Swaney, D. P.: The Coastal Zone — a Domain of Global Interactions, in: *Coastal Fluxes in the Anthropocene: The Land–Ocean Interactions in the Coastal Zone Project of the International Geosphere–Biosphere Programme*, edited by Crossland, C. J., Kremer, H. H., Lindeboom, H. J., Marshall Crossland, J. I., and Le Tissier, M. D. A., *Global Change — The IGBP Series*, pp. 1–37, Springer, Berlin, Heidelberg, 2005.
- De La Rocha, C. L. and Passow, U.: *The Biological Pump*, in: *Treatise on Geochemistry (Second Edition)*, edited by Holland, H. D. and Turekian, K. K., pp. 93–122, Elsevier, Oxford, 2014.
- 305 Derot, J., Schmitt, F. G., Gentilhomme, V., and Morin, P.: Correlation between Long-Term Marine Temperature Time Series from the Eastern and Western English Channel: Scaling Analysis Using Empirical Mode Decomposition, *Comptes Rendus Geoscience*, 348, 343–349, <https://doi.org/10.1016/j.crte.2015.12.001>, 2016.
- Drupp, P., De Carlo, E. H., Mackenzie, F. T., Bienfang, P., and Sabine, C. L.: Nutrient Inputs, Phytoplankton Response, and CO<sub>2</sub> Variations in a Semi-Enclosed Subtropical Embayment, Kaneohe Bay, Hawaii, *Aquatic Geochemistry*, 17, 473–498, <https://doi.org/10.1007/s10498-010-9115-y>, 2011.
- Emerson, S. R. and Hamme, R. C.: *Chemical Oceanography*, Cambridge University Press, 2022.
- Falkowski, P., Scholes, R. J., Boyle, E., Canadell, J., Canfield, D., Elser, J., Gruber, N., Hibbard, K., Högberg, P., Linder, S., Mackenzie, F. T., Moore III, B., Pedersen, T., Rosenthal, Y., Seitzinger, S., Smetacek, V., and Steffen, W.: The Global Carbon Cycle: A Test of Our Knowledge of Earth as a System, *Science*, 290, 291–296, <https://doi.org/10.1126/science.290.5490.291>, 2000.
- 315 Flandrin, P., Rilling, G., and Goncalves, P.: Empirical Mode Decomposition as a Filter Bank, *IEEE signal processing letters*, 11, 112–114, 2004.
- Friedlingstein, P., O'Sullivan, M., Jones, M. W., Andrew, R. M., Bakker, D. C. E., Hauck, J., Landschützer, P., Le Quéré, C., Luijkx, I. T., Peters, G. P., Peters, W., Pongratz, J., Schwingshackl, C., Sitch, S., Canadell, J. G., Ciais, P., Jackson, R. B., Alin, S. R., Anthoni, P., Barbero, L., Bates, N. R., Becker, M., Bellouin, N., Decharme, B., Bopp, L., Brasika, I. B. M., Cadule, P., Chamberlain, M. A., Chandra, N., Chau, T.-T.-T., Chevallier, F., Chini, L. P., Cronin, M., Dou, X., Enyo, K., Evans, W., Falk, S., Feely, R. A., Feng, L., Ford, D. J., Gasser, T., Ghattas, J., Gkritzalis, T., Grassi, G., Gregor, L., Gruber, N., Gürses, Ö., Harris, I., Hefner, M., Heinke, J., Houghton, R. A.,



- Hurtt, G. C., Iida, Y., Ilyina, T., Jacobson, A. R., Jain, A., Jarníková, T., Jersild, A., Jiang, F., Jin, Z., Joos, F., Kato, E., Keeling, R. F., Kennedy, D., Klein Goldewijk, K., Knauer, J., Korsbakken, J. I., Körtzinger, A., Lan, X., Lefèvre, N., Li, H., Liu, J., Liu, Z., Ma, L.,  
325 Marland, G., Mayot, N., McGuire, P. C., McKinley, G. A., Meyer, G., Morgan, E. J., Munro, D. R., Nakaoka, S.-I., Niwa, Y., O'Brien, K. M., Olsen, A., Omar, A. M., Ono, T., Paulsen, M., Pierrot, D., Pockock, K., Poulter, B., Powis, C. M., Rehder, G., Resplandy, L., Robertson, E., Rödenbeck, C., Rosan, T. M., Schwinger, J., Séférian, R., Smallman, T. L., Smith, S. M., Sospedra-Alfonso, R., Sun, Q., Sutton, A. J., Sweeney, C., Takao, S., Tans, P. P., Tian, H., Tilbrook, B., Tsujino, H., Tubiello, F., van der Werf, G. R., van Ooijen, E., Wanninkhof, R., Watanabe, M., Wimart-Rousseau, C., Yang, D., Yang, X., Yuan, W., Yue, X., Zaehle, S., Zeng, J., and Zheng, B.: Global  
330 Carbon Budget 2023, *Earth System Science Data*, 15, 5301–5369, <https://doi.org/10.5194/essd-15-5301-2023>, 2023.
- Frisch, U.: *Turbulence: The Legacy of A. N. Kolmogorov*, Cambridge University Press, 1995.
- Gao, Y., Schmitt, F. G., Hu, J., and Huang, Y.: Scaling Analysis of the China France Oceanography Satellite Along-Track Wind and Wave Data, *Journal of Geophysical Research: Oceans*, 126, e2020JC017119, <https://doi.org/10.1029/2020JC017119>, 2021.
- Gao, Z., Liu, H., Arntzen, E., Mcfarland, D. P., Chen, X., and Huang, M.: Uncertainties in Turbulent Statistics and Fluxes of CO<sub>2</sub> Associated  
335 With Density Effect Corrections, *Geophysical Research Letters*, 47, e88859, <https://doi.org/10.1029/2020GL088859>, 2020.
- Henson, S., Le Moigne, F., and Giering, S.: Drivers of Carbon Export Efficiency in the Global Ocean, *Global Biogeochemical Cycles*, 33, 891–903, <https://doi.org/10.1029/2018GB006158>, 2019.
- Hernández-Carrasco, I., Sudre, J., Garçon, V., Yahia, H., Garbe, C., Paulmier, A., Dewitte, B., Illig, S., Dadou, I., González-Dávila, M., and Santana-Casiano, J. M.: Reconstruction of Super-Resolution Ocean *p*CO<sub>2</sub> and Air–Sea Fluxes of CO<sub>2</sub> from Satellite Imagery in the  
340 Southeastern Atlantic, *Biogeosciences*, 12, 5229–5245, <https://doi.org/10.5194/bg-12-5229-2015>, 2015.
- Hernández-Carrasco, I., Garçon, V., Sudre, J., Garbe, C., and Yahia, H.: Increasing the Resolution of Ocean *p*CO<sub>2</sub> Maps in the South Eastern Atlantic Ocean Merging Multifractal Satellite-Derived Ocean Variables, *IEEE Transactions on Geoscience and Remote Sensing*, 56, 6596–6610, <https://doi.org/10.1109/TGRS.2018.2840526>, 2018.
- Huang, N. E., Shen, Z., Long, S. R., Wu, M. C., Shih, H. H., Zheng, Q., Yen, N.-C., Tung, C. C., and Liu, H. H.: The Empirical Mode  
345 Decomposition and the Hilbert Spectrum for Nonlinear and Non-Stationary Time Series Analysis, *Proceedings of the Royal Society of London. Series A: mathematical, physical and engineering sciences*, 454, 903–995, 1998.
- Huang, N. E., Shen, Z., and Long, S. R.: A New View of Nonlinear Water Waves: The Hilbert Spectrum, *Annual review of fluid mechanics*, 31, 417–457, 1999.
- Huang, Y. X., Schmitt, F. G., Lu, Z. M., and Liu, Y. L.: An Amplitude-Frequency Study of Turbulent Scaling Intermittency Using Empirical  
350 Mode Decomposition and Hilbert Spectral Analysis, *Europhysics Letters*, 84, 40010, 2008.
- Huang, Y. X., Schmitt, F. G., Hermand, J.-P., Gagne, Y., Lu, Z. M., and Liu, Y. L.: Arbitrary-Order Hilbert Spectral Analysis for Time Series Possessing Scaling Statistics: Comparison Study with Detrended Fluctuation Analysis and Wavelet Leaders, *Physical Review E*, 84, 016208, <https://doi.org/10.1103/PhysRevE.84.016208>, 2011.
- Jin, M., Deal, C., Wang, J., Alexander, V., Gradinger, R., Saitoh, S.-i., Iida, T., Wan, Z., and Stabeno, P.: Ice-Associated Phytoplankton  
355 Blooms in the Southeastern Bering Sea, *Geophysical Research Letters*, 34, <https://doi.org/10.1029/2006GL028849>, 2007.
- Katul, G. G., Chu, C. R., Parlange, M. B., Albertson, J. D., and Ortenburger, T. A.: Low-Wavenumber Spectral Characteristics of Velocity and Temperature in the Atmospheric Surface Layer, *Journal of Geophysical Research: Atmospheres*, 100, 14243–14255, <https://doi.org/10.1029/94JD02616>, 1995.



- Kealoha, A. K., Shamberger, K. E. F., DiMarco, S. F., Thyng, K. M., Hetland, R. D., Manzello, D. P., Slowey, N. C., and Enochs, I. C.: Surface  
360 Water CO<sub>2</sub> Variability in the Gulf of Mexico (1996–2017), *Scientific Reports*, 10, 12 279, <https://doi.org/10.1038/s41598-020-68924-0>,  
2020.
- Keenan, T., Baker, I., Barr, A., Ciais, P., Davis, K., Dietze, M., Dragoni, D., Gough, C. M., Grant, R., Hollinger, D., Hufkens, K., Poul-  
ter, B., McCaughey, H., Raczka, B., Ryu, Y., Schaefer, K., Tian, H., Verbeeck, H., Zhao, M., and Richardson, A. D.: Terrestrial Bio-  
sphere Model Performance for Inter-Annual Variability of Land-Atmosphere CO<sub>2</sub> Exchange, *Global Change Biology*, 18, 1971–1987,  
365 <https://doi.org/10.1111/j.1365-2486.2012.02678.x>, 2012.
- Kolmogorov, A. N.: On Degeneration (Decay) of Isotropic Turbulence in an Incompressible Viscous Liquid, in: *Dokl. Akad. Nauk SSSR*,  
vol. 31, pp. 538–540, 1941.
- Kolmogorov, A. N.: A Refinement of Previous Hypotheses Concerning the Local Structure of Turbulence in a Viscous Incompressible Fluid  
at High Reynolds Number, *Journal of Fluid Mechanics*, 13, 82–85, <https://doi.org/10.1017/S0022112062000518>, 1962.
- 370 Kwiatkowski, L., Torres, O., Aumont, O., and Orr, J. C.: Modified Future Diurnal Variability of the Global Surface Ocean CO<sub>2</sub> System,  
*Global change biology*, 29, 982–997, <https://doi.org/10.1111/gcb.16514>, 2023.
- Landschützer, P., Gruber, N., and Bakker, D. C. E.: Decadal Variations and Trends of the Global Ocean Carbon Sink, *Global Biogeochemical  
Cycles*, 30, 1396–1417, <https://doi.org/10.1002/2015GB005359>, 2016.
- Liu, Z., Deng, Z., Davis, S. J., Giron, C., and Ciais, P.: Monitoring Global Carbon Emissions in 2021, *Nature Reviews Earth & Environment*,  
375 3, 217–219, <https://doi.org/10.1038/s43017-022-00285-w>, 2022.
- Obukhov, A. M.: The Structure of the Temperature Field in a Turbulent Flow, *IZv. Akad. Nauk SSSR. Ser. Geogr. Geofia*, 13, 1949.
- Ohtaki, E.: On the Similarity in Atmospheric Fluctuations of Carbon Dioxide, Water Vapor and Temperature over Vegetated Fields,  
*Boundary-Layer Meteorology*, 32, 25–37, <https://doi.org/10.1007/BF00120712>, 1985.
- Ohtaki, E., Tsukamoto, O., Iwatani, Y., and Mitsuta, Y.: Measurements of the Carbon Dioxide Flux over the Ocean, *Journal of the Meteor-  
380 ological Society of Japan. Ser. II*, 67, 541–554, [https://doi.org/10.2151/jmsj1965.67.4\\_541](https://doi.org/10.2151/jmsj1965.67.4_541), 1989.
- Pathak, M., Slade, R., Shukla, P., Skea, J., Pichs-Madruga, R., and Ürge-Vorsatz, D.: Technical Summary, *Climate Change 2022: Mitigation  
of Climate Change. Contribution of Working Group III to the Sixth Assessment Report of the Intergovernmental Panel on Climate Change*,  
[P.R. Shukla, J. Skea, R. Slade, A. Al Khourdajie, R. van Diemen, D. McCollum, M. Pathak, S. Some, P. Vyas, R. Fradera, M. Belkacemi,  
A. Hasija, G. Lisboa, S. Luz, J. Malley, (eds.)], <https://doi.org/10.1017/9781009157926.002>, 2022.
- 385 Pritchard, D. T. and Currie, J. A.: Diffusion of Coefficients of Carbon Dioxide, Nitrous Oxide, Ethylene and Ethane in Air and Their  
Measurement, *Journal of Soil Science*, 33, 175–184, <https://doi.org/10.1111/j.1365-2389.1982.tb01757.x>, 1982.
- Roland, M., Serrano-Ortiz, P., Kowalski, A. S., Goddérís, Y., Sánchez-Cañete, E. P., Ciais, P., Domingo, F., Cuezva, S., Sanchez-Moral, S.,  
Longdoz, B., Yakir, D., Van Grieken, R., Schott, J., Cardell, C., and Janssens, I. A.: Atmospheric Turbulence Triggers Pronounced Diel  
Pattern in Karst Carbonate Geochemistry, *Biogeosciences*, 10, 5009–5017, <https://doi.org/10.5194/bg-10-5009-2013>, 2013.
- 390 Sahlée, E., Smedman, A.-S., Rutgersson, A., and Högström, U.: Spectra of CO<sub>2</sub> and Water Vapour in the Marine Atmospheric Surface Layer,  
*Boundary-Layer Meteorology*, 126, 279–295, <https://doi.org/10.1007/s10546-007-9230-5>, 2008.
- Sarmiento, J. L. and Gruber, N.: Sinks for Anthropogenic Carbon, *Physics Today*, 55, 30–36, <https://doi.org/10.1063/1.1510279>, 2002.
- Schmitt, F., Schertzer, D., Lovejoy, S., and Brunet, Y.: Empirical Study of Multifractal Phase Transitions in Atmospheric Turbulence, *Non-  
linear Processes in Geophysics*, 1, 95–104, <https://doi.org/10.5194/npg-1-95-1994>, 1994.
- 395 Schmitt, F., Schertzer, D., Lovejoy, S., and Brunet, Y.: Multifractal Temperature and Flux of Temperature Variance in Fully Developed  
Turbulence, *Europhysics Letters*, 34, 195, <https://doi.org/10.1209/epl/i1996-00438-4>, 1996.



- Schmitt, F. G.: Linking Eulerian and Lagrangian Structure Functions' Scaling Exponents in Turbulence, *Physica A: Statistical Mechanics and its Applications*, 368, 377–386, <https://doi.org/10.1016/j.physa.2005.12.028>, 2006.
- Schmitt, F. G.: Gusts in Intermittent Wind Turbulence and the Dynamics of Their Recurrent Times, in: *Wind Energy*, edited by Peinke, J., Schaumann, P., and Barth, S., pp. 73–79, Springer Berlin Heidelberg, Berlin, Heidelberg, 2007.
- 400 Schmitt, F. G. and Huang, Y.: *Stochastic Analysis of Scaling Time Series: From Turbulence Theory to Applications*, Cambridge University Press, 2016.
- Schmitt, F. G., Dur, G., Souissi, S., and Brizard Zongo, S.: Statistical Properties of Turbidity, Oxygen and pH Fluctuations in the Seine River Estuary (France), *Physica A: Statistical Mechanics and its Applications*, 387, 6613–6623, <https://doi.org/10.1016/j.physa.2008.08.026>,  
405 2008.
- Seuront, L., Schmitt, F., Lagadeuc, Y., Schertzer, D., Lovejoy, S., and Frontier, S.: Multifractal Analysis of Phytoplankton Biomass and Temperature in the Ocean, *Geophysical Research Letters*, 23, 3591–3594, <https://doi.org/10.1029/96GL03473>, 1996.
- Stabeno, P., Napp, J., Mordy, C., and Whitlege, T.: Factors Influencing Physical Structure and Lower Trophic Levels of the Eastern Bering Sea Shelf in 2005: Sea Ice, Tides and Winds, *Progress in Oceanography*, 85, 180–196, <https://doi.org/10.1016/j.pocean.2010.02.010>, 2010.
- 410 Sutton, A. J., Sabine, C. L., Maenner-Jones, S., Lawrence-Slavas, N., Meinig, C., Feely, R. A., Mathis, J. T., Musielewicz, S., Bott, R., and McLain, P. D.: A High-Frequency Atmospheric and Seawater  $p\text{CO}_2$  Data Set from 14 Open-Ocean Sites Using a Moored Autonomous System, *Earth System Science Data*, 6, 353–366, 2014.
- Sutton, A. J., Feely, R. A., Maenner-Jones, S., Musielwicz, S., Osborne, J., Dietrich, C., Monacci, N., Cross, J., Bott, R., Kozyr, A., Anderson, A. J., Bates, N. R., Cai, W.-J., Cronin, M. F., De Carlo, E. H., Hales, B., Howden, S. D., Lee, C. M., Manzello, D. P., McPhaden,  
415 M. J., Meléndez, M., Mickett, J. B., Newton, J. A., Noakes, S. E., Noh, J. H., Olafsdottir, S. R., Salisbury, J. E., Send, U., Trull, T. W., Vandemark, D. C., and Weller, R. A.: Autonomous Seawater  $p\text{CO}_2$  and pH Time Series from 40 Surface Buoys and the Emergence of Anthropogenic Trends, *Earth System Science Data*, 11, 421–439, <https://doi.org/10.5194/essd-11-421-2019>, 2019.
- Thorpe, S. A.: *The Turbulent Ocean*, Cambridge University Press, Cambridge, 2005.
- Thorpe, S. A.: *An Introduction to Ocean Turbulence*, Cambridge University Press, Cambridge, 2007.
- 420 Torres, O., Kwiatkowski, L., Sutton, A. J., Dorey, N., and Orr, J. C.: Characterizing Mean and Extreme Diurnal Variability of Ocean  $\text{CO}_2$  System Variables Across Marine Environments, *Geophysical Research Letters*, 48, e2020GL090228, <https://doi.org/10.1029/2020GL090228>, 2021.
- Turk, D., Zappa, C. J., Meinen, C. S., Christian, J. R., Ho, D. T., Dickson, A. G., and McGillis, W. R.: Rain Impacts on  $\text{CO}_2$  Exchange in the Western Equatorial Pacific Ocean, *Geophysical Research Letters*, 37, <https://doi.org/10.1029/2010GL045520>, 2010.
- 425 Walker, N. D., Wiseman, Jr., W. J., Rouse, Jr., L. J., and Babin, A.: Effects of River Discharge, Wind Stress, and Slope Eddies on Circulation and the Satellite-Observed Structure of the Mississippi River Plume, *Journal of Coastal Research*, 21, 1228–1244, <https://doi.org/10.2112/04-0347.1>, 2005.
- Wanninkhof, R.: Relationship between Wind Speed and Gas Exchange over the Ocean Revisited, *Limnology and Oceanography: Methods*, 12, 351–362, 2014.
- 430 Yamamoto, A., Abe-Ouchi, A., and Yamanaka, Y.: Long-Term Response of Oceanic Carbon Uptake to Global Warming via Physical and Biological Pumps, *Biogeosciences*, 15, 4163–4180, <https://doi.org/10.5194/bg-15-4163-2018>, 2018.
- Yue, X.-L. and Gao, Q.-X.: Contributions of Natural Systems and Human Activity to Greenhouse Gas Emissions, *Advances in Climate Change Research*, 9, 243–252, <https://doi.org/10.1016/j.accre.2018.12.003>, 2018.



- 435 Zhang, M., Cheng, Y., Bao, Y., Zhao, C., Wang, G., Zhang, Y., Song, Z., Wu, Z., and Qiao, F.: Seasonal to Decadal Spatiotemporal Variations of the Global Ocean Carbon Sink, *Global Change Biology*, 28, 1786–1797, <https://doi.org/10.1111/gcb.16031>, 2022.
- Zongo, S. B. and Schmitt, F. G.: Scaling Properties of pH Fluctuations in Coastal Waters of the English Channel: pH as a Turbulent Active Scalar, *Nonlinear Processes in Geophysics*, 18, 829–839, <https://doi.org/10.5194/npg-18-829-2011>, 2011.